Progress Report, 2008-09, Southern California Earthquake Center

Dynamics of Rupture Branching for the Solitario Canyon Fault and other Fault Junction Problems

Renata Dmowska (Co-PI), and James R. Rice (PI)
Harvard University, Cambridge, MA 02138
FY '08 SCEC Project #08077, $45,000 for 1 Feb 2008 to 31 Jan 2009

Report prepared 31 March 2009

Recent reports related to theme of this project:

DeDontney, N. , E. L. Templeton, H. Bhat, R. Dmowska and J. R. Rice, "Criteria for seismic splay fault activation during subduction earthquakes", Eos Trans. AGU, 89(53), Fall Meet. Suppl., Abstract T11D-02, 2008.

Rice, J. R., "How granulated/cracked fault border zones, and their pore fluids, interact with earthquake rupture dynamics", Conference on *Fault Zones: Structure, Geomechanics and Fluid Flow*, The Geological Society, London, 16-18 September 2008.

Templeton, A. Baudet, H. S. Bhat, R. Dmowska, J. R. Rice, A. J. Rosakis, and C.-E. Rousseau, "Finite element simulations of dynamic shear rupture experiments and dynamic path selection along kinked and branched faults", submitted to *Journal of Geophysical Research*, October 2008

Templeton, E. L., H. S. Bhat, R. Dmowska and J. R. Rice, "Dynamic Rupture Through a Branched Fault Configuration at Yucca Mountain, NV", Seismological Society of America, Annual Meeting, 16-18 April 2008, Santa Fe, NM.

Templeton, E. L., H. S. Bhat, R. Dmowska and J. R. Rice, "Dynamic Rupture Through Branched Fault Configurations With Off-fault Inelastic Response", Eos Trans. AGU, 89(53), Fall Meet. Suppl., Abstract S51D-1766, 2008.

Progress

We studied dynamic rupture with fault branching along the Solitario Canyon Fault (SCF) bordering Yucca Mountain (YM), Nevada (Fig. 1), in a configuration of specific interest for the Extreme Ground Motion project. In concert with that, we also initiated more general studies on rupture through (or arrest at) complex fault junctions that involve branches and damaged fault-bordering zones. The studies allowing for Mohr-Coulomb type elastic-plastic response in the simplified Drucker-prager formulation. The SCF/YM configuration was addressed in a manner appropriate to normal faulting environments, to identify conditions under which known branching faults from the SCF would be activated seismically, and what that would mean for strong ground motions at the proposed repository site. We also completed a multi-year study of correlation of our theoretical, finite-element based, models of rupture along kinked and branched fault paths with extensive laboratory studies of such configurations by Ares Rosakis at Caltech and his former co-worker Carl Rousseau, now at the University of Rhode Island.

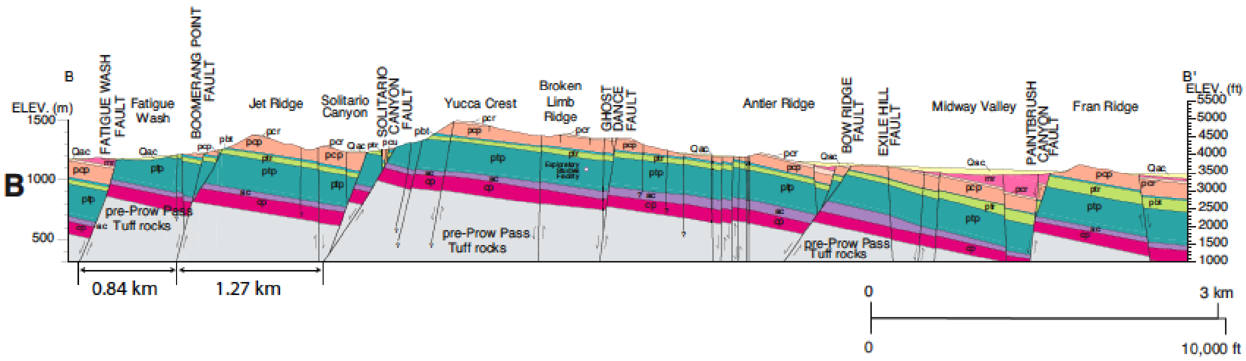

Fig. 1. Cross sectional view of faults in the vicinity of Yucca Mountain showing steeply Eastward dipping normal faults west of the Solitario Canyon Fault [Potter et al., 2004].

Solitario Canyon Fault at Yucca Mountain: Potter et al. [2004] describe the geometry of the Yucca Mountain region as consisting of (1) block-bounding normal faults, spaced 1-4 km apart, (2) northwest-striking relay faults linking displacement between the block bounding faults, (3) discontinuous intra-block faults, and (4) mesoscopic fracture network. We seek to gain insight into the interaction between the major block-bounding faults in the Yucca Mountain region during a dynamic rupture event. Branching and jumping during a seismic event could have major implications for the rupture velocity and resulting ground motions.

The major block bounding faults, which include the SCF, Windy Wash Fault (WWF), and Fatigue Wash Fault (FWF), were active at Yucca Mountain during and after eruption of the 12.8-12.7 Ma Paintbrush group. An issue is whether the next seismic rupture along SCF would be expected to also induce rupture along the WWF and/or the FWF, and how that impacts ground motions at the proposed storage site. Potter et al. 1999 and Potter et al. 2004 give maps and cross section views of the faults in the area surrounding Yucca Mountain, as partially shown here in Fig. 1. The cross section B shows that the SCF has a dip of ~57^o and the FWF has a dip of ~69^o between 1-1.5 km depth, and are separated by a distance of 2.3 km at an elevation of 1150 m. If the SCF and FWF continue to dip at those angles, they would intersect at a depth of 9.2 km. We will investigated a range of normal fault geometries, with branch angles that would seem plausible in view of the known near-surface features, for the major block bounding faults surrounding YM to determine whether branch activation is likely in that area. The principal pre-stress direction is plausibly taken as vertical but we will also investigate the effects of modest variations in that as driven by topography and coordinated past shear on the bounding faults.

Kame et al. [2003] addressed, using a boundary integral equation (BIE) method, whether a branch fault off a rupturing main fault would be taken or not, and if rupture would abandon the main fault or continue on it as well. They identified how that depends on the initial stress state (especially on the angle Ψ that the most compressive principal stress makes with the fault), the branch angle ϕ, and the rupture velocity v_r along the main fault at the branch junction. We have turned to the finite element (FE) method, in the form of the ABAQUS/Explicit program, for these studies. Using FE, we have been able to closely reproduce the elastic results of Kame et al. [2003] on branching to which we have thus far compared, which includes cases of shallow branch angles ϕ that would be considered demanding for FE methodology.

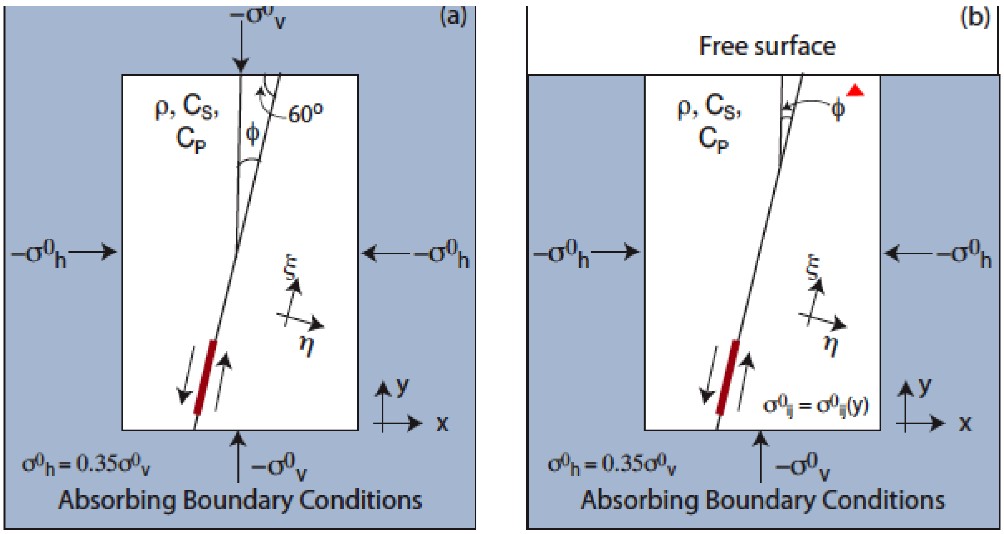

Fig. 2. Schematic of finite element models, Solitario Canyon Fault scenario study, used for the (a) constant pre-stress branching study, and (b) depth-dependent pre-stress.

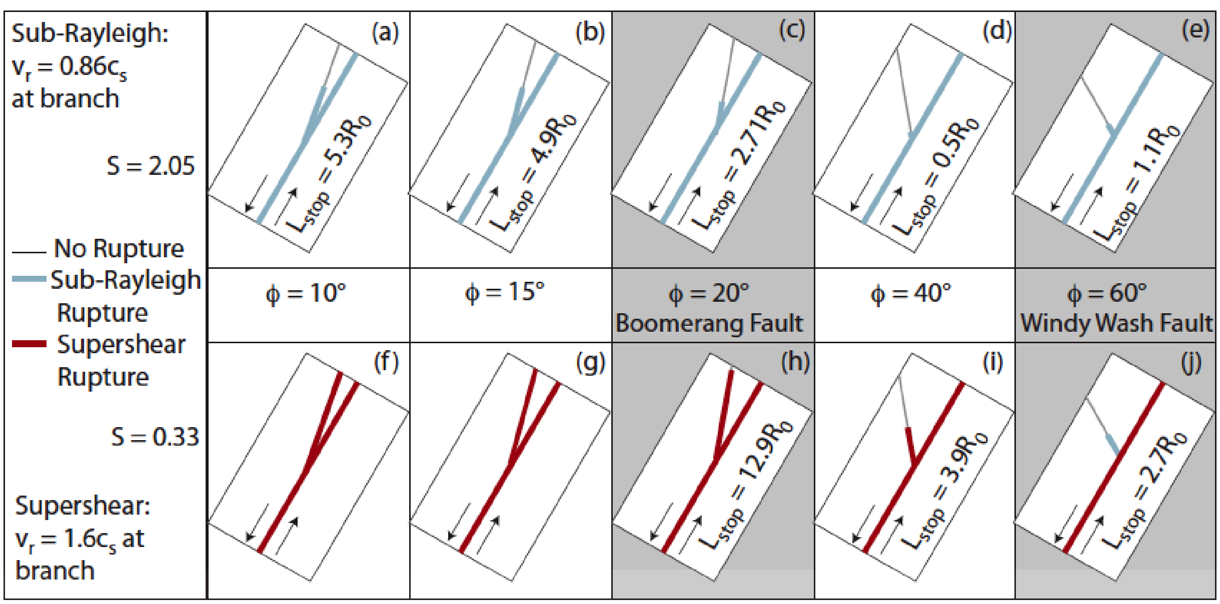

Fig. 3. Branching results, constant pre-stress, for branch angles ranging from 10º to 60º; elastic medium.

In the branching configurations examined to model possible Yucca Mountain rupture scenarios, we considered the effects of depth-dependent stresses and free-surface effects, Fig. 2, the effects of elastic, Fig. 3, versus inelastic, Fig. 4, off-fault deformation (in the form of pressuredependent yielding), and radiated ground motions in different scenarios (with/without branch activation, plasticity) at the proposed repository site, Fig. 5.

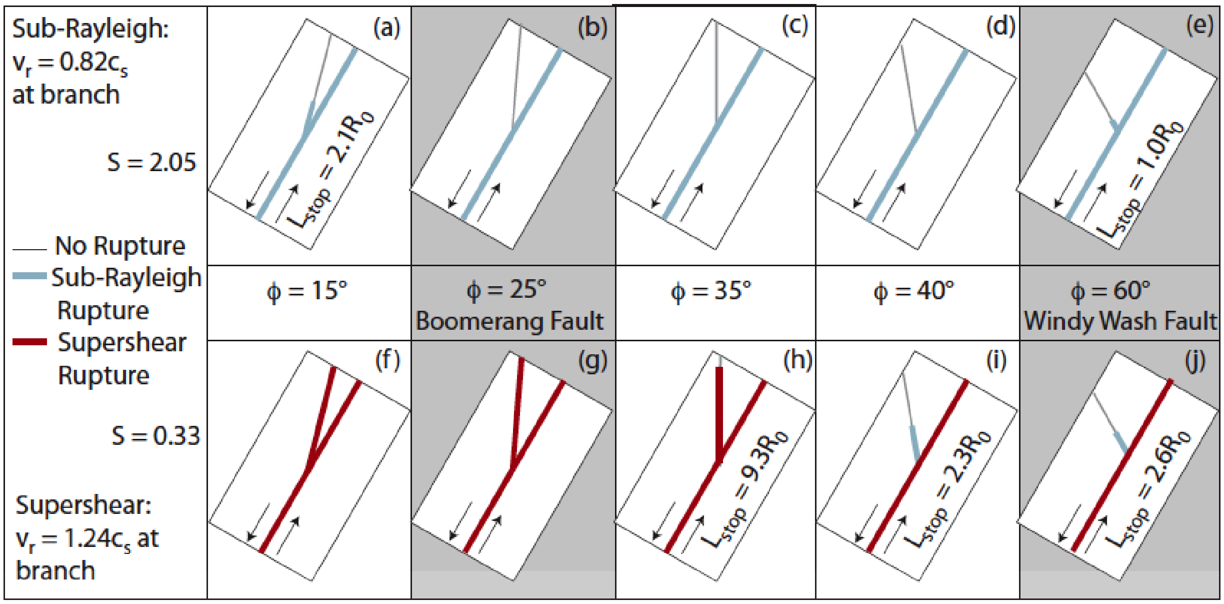

Fig. 4. Branching results for constant pre-stress states with inelastic off-fault material response allowed.

Depth-Dependent Pre-Stress Results: The constant pre-stress state analyses suggested that the most likely scenario for activation of a fault branch on the hanging wall of the Solitario Canyon Fault is a steeply Eastward dipping branch with an angle of less than 25º between the branched fault and the SCF. Using the finite element model, the effects of branched fault activation on the ground motions at the potential repository site, 1 km west of the SCF and 200 km below the free surface, were determined. A splay fault dipping 80º to the west intersecting the Solitario Canyon Fault at 3 km depth was considered. Rupture was initiated at 11 km depth by a sudden drop in shear stress.

The slip-weakening distance D_c was taken as 0.1m, which corresponds to an R_0 of 60 m at 8 km depth. Along the fault, the node spacing was 14 m. Both the elastic and elastic-plastic constant stress model results indicated that supershear rupture is the best candidate for branch fault activation.

First, effects of branch fault activation with elastic off-fault material response were considered. Rupture began at depth along the SCF and propagates at a supershear velocity updip reaching the splay fault at a depth of 3 km with a propagation speed of 1.66 c_s. Activation of the splay fault occurs, and supershear rupture occurs along the splay fault at 1.74 c_s. Figs. 5 (a) and (b) show the horizontal and vertical velocities at the repository site for the branch activation (blue) and for a reference case with no branch activation (black). The ground motions were similar until arrival of motions from rupture along the branched fault. There is a second large peak in vertical ground velocities at the repository site corresponding the Mach front from the supershear rupture along the splay fault reaching the repository site.

Next, the effects of off-fault inelastic deformation were included, taking Mohr-Coulomb parameters μ (= sin ϕ) = 0.7, cohesion = 7 MPa, and with no plastic dilation included [consistent with Andrews]. Figs. 5 (c) and (d) show the ground motions produced by branch activation in an elastic (blue) and elastic-plastic (red) responding materials. The peak horizontal ground velocities were reduced by 15% and the vertical peak velocities by 19%.

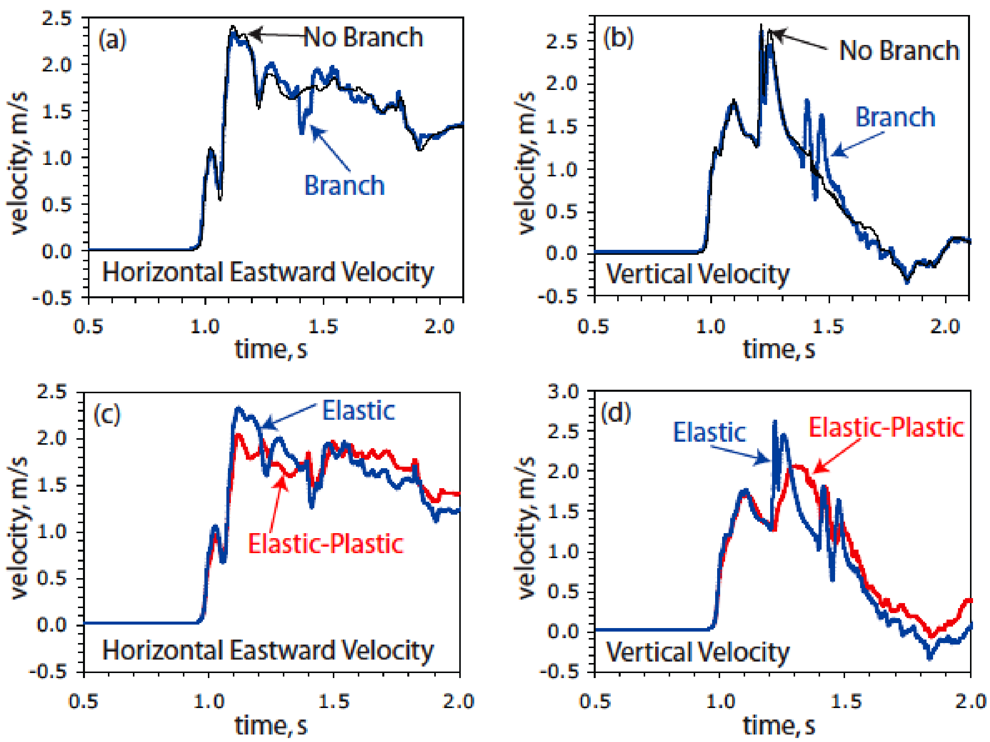

Fig. 5. Effects of (a-b) branch activation and (c-d) elastic-plastic off-fault material response on vertical and horizontal ground velocities at the proposed repository site (1 km east of the Solitario Canyon Fault 200 m below the free surface) during a supershear rupture propagation along the SCF.

Fig. 6 shows a schematic of the set-up of the Rouseau and Rosakis [2003, 2009] experiments on which we have collaborated to test theoretical concepts and try to explain observations. Fig. 7 shows the specimen configurations to represent either kinks or branches in a fault system. The specimens were cut along bent or branched paths and then weakly glued back together everywhere except along a starter notch near the impact site. In the finite-element simulations, we could not model the impact of the steel buffers with the much more compliant Homalite-100 plates (chosen for their photoelastic properties), because the vastly different waves speeds required too large a gradation in element size to meet a CFL criterion for a necessarily uniform time step throughout the domain. The impact was therefore represented by an imposed horizontal velocity history at the border with the buffer, correlated against strain gauge measurements in the Homalite just inward from that border.

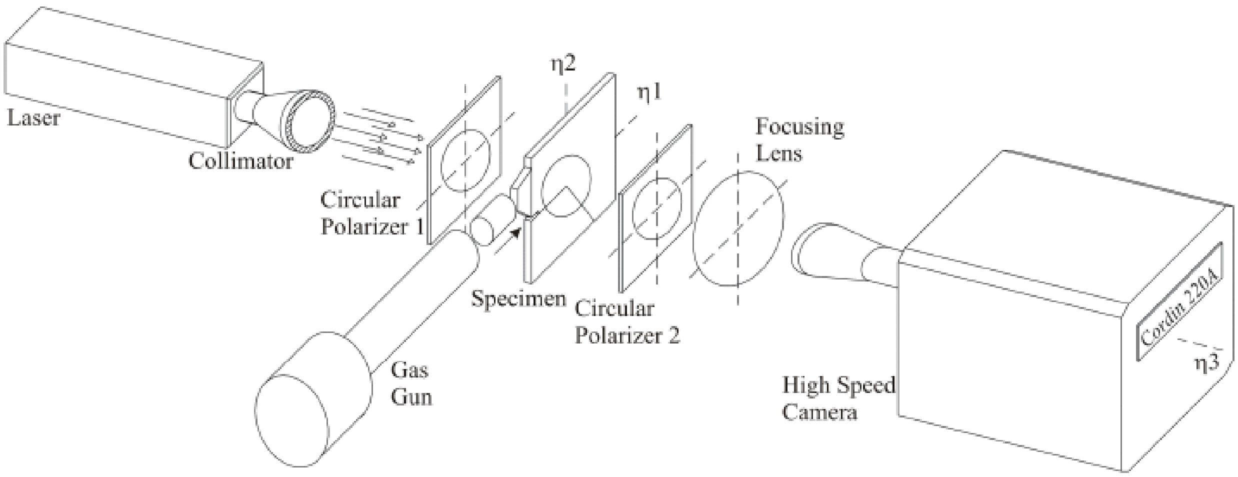

Fig. 6. Schematic of the experimental dynamic photoelastic setup and high-speed camera from the experiments of Rousseau and Rosakis [2003, 2009], for a specimen with a kinked weakened path (~fault).

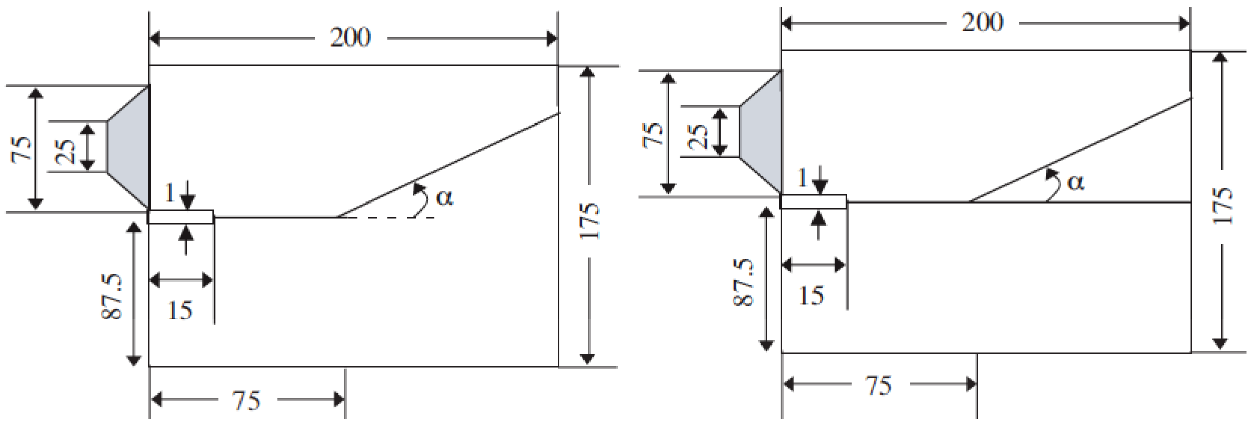

Fig. 7. Geometry of the 5 mm thick Homalite-100 plate with steel buffer used in (left) kinked and (right) branched fault experiments. All dimensions are in mm. Positive and negative kink and branch fault inclination angles α were considered. For positive α, the secondary fault is on the compressional side of rupture along the main fault, that is, the side experiencing compressional fault parallel strain ahead of the rupture. The secondary fault is on the extensional side for negative α.

We found that dynamic explicit 2D plane-stress finite element analyses with a simple linear slip-weakening description of cohesive and frictional strength of the bonded interfaces could reproduce the qualitative rupture behavior past the bend and branch junctions in most cases and reproduce the principal features revealed by the high-speed photographs of the dynamic isochromatic fringe line patterns; Fig. 8. There is also good agreement between the numerical and experimental crack tip positions during rupture. The finite element results provide additional insight into differences in the amount of slip accumulation occurring on the main horizontal fault versus that occurring on the inclined fault bends or branched faults, which differences are not readily characterized in the experiments, and they indicate that slip along the inclined faults can be substantially less, even with apparently vigorous rupture propagation, than slip along the the main fault. Differences between the numerical and experimental results exist for cases with a bend or branch along the extensional side, perhaps due, at least in part, to mixed mode rupture micro-crack formation in the bulk during the experiments which cannot be modeled within the simple cohesive and frictional laws implemented in this numerical study. Future studies could incorporate a tensile component of fault strength in the slip-weakening description to (we assume) better match the experimental results.

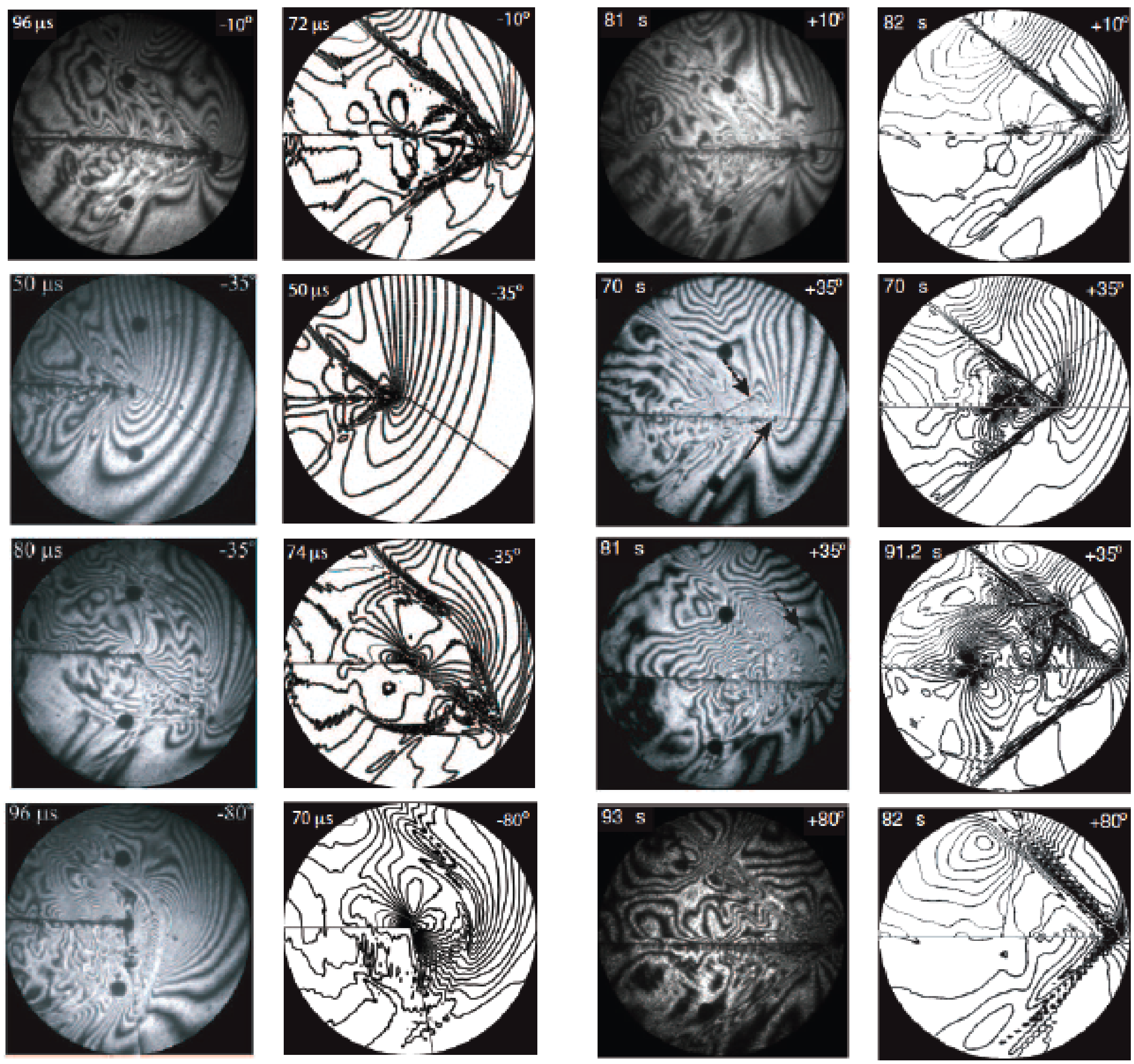

Fig. 8. Comparison between isochromatic fringe patterns observed by high speed photography (1st and 3rd columns) with the fringe patterns as computed from the stress field in the dynamic rupture simulations (2nd and 4th columns). Results on the left (1st and 2nd columns) are for specimens with kinked weakened paths at various angles to the extensional side. Those on the right (3rd and 4th columns) are for branched weakened paths, with the inclined branch at various angles to the compressional side.